Sciencexpress Research Article

# Calibrating the End-Permian Mass Extinction

Shu-zhong Shen,[1]* James L. Crowley,[2,3] Yue Wang,[1]* Samuel A. Bowring,[2]* Douglas H. Erwin,[4,5] Peter M. Sadler,[6] Chang-qun Cao,[1] Daniel H. Rothman,[7] Charles M. Henderson,[8] Jahandar Ramezani,[2] Hua Zhang,[1] Yanan Shen,[1,9] Xiang-dong Wang,[1] Wei Wang,[1] Lin Mu,[1] Wen-zhong Li,[1,10] Yue-gang Tang,[11] Xiao-lei Liu,[1,12] Lu-jun Liu,[1] Yong Zeng,[13] Yao-fa Jiang,[14] Yu-gan Jin[1]

[1]LPS, Nanjing Institute of Geology and Palaeontology, 39 East Beijing Road, Nanjing 210008, China. [2]Department of Earth, Atmospheric and Planetary Sciences, Massachusetts Institute of Technology, 77 Massachusetts Avenue, Cambridge, MA 02130, USA. [3]Department of Geosciences, Boise State University, 1910 University Drive, Boise, ID 83725, USA. [4]Department of Paleobiology, MRC-121, National Museum of Natural History, Washington D.C. USA 20013-7012, USA. [5]Santa Fe Institute, 1399 Hyde Park Road, Santa Fe, NM 87591, USA. [6]Department of Earth Sciences, University of California, Riverside, CA 92521, USA. [7]Lorenz Center, Massachusetts Institute of Technology, Cambridge, MA 02139 USA. [8]Department of Geoscience, University of Calgary, Calgary, AB, Canada T2N 1N4. [9]CAS Key Laboratory of Crust-Mantle Materials and Environments, School of Earth and Space Sciences, University of Science and Technology of China, Hefei 230026, China. [10]School of Life and Environmental Sciences, Deakin University, Melbourne Campus, 221 Burwood Highway, Burwood, Victoria 3125, Australia. [11]Department of Geology, China University of Mining and Technology, Beijing Campus, D-11 Xueyuan Road, Beijing 100083, China. [12] University of Bremen, Leobener Street, Marum; Room 2520, 28359 Bremen, Germany. [13]School of Resources and Geosciences, China University of Mining and Technology, Xuzhou, Jiangsu 221008, China. [14]Jiangsu Geological Survey of Architectural Institute, Xuzhou, Jiangsu 221116, China.

*To whom correspondence should be addressed: E-mail: sbowring@mit.edu (S.A.B.); yuewang@nigpas.ac.cn (Y.W.); szshen@nigpas.ac.cn (S.Z.S.)

**The end-Permian mass extinction was the most severe biodiversity crisis in earth history. To better constrain the timing, and ultimately the causes of this event, we collected a suite of geochronologic, isotopic and biostratigraphic data on several well-preserved sedimentary sections in South China. High-precision U-Pb dating reveals that the extinction peak occurred just before 252.28 ± 0.08 Ma, following a decline of 2‰ in $\delta^{13}C$ over 90,000 years, and coincided with a $\delta^{13}C$ excursion of -5‰ that is estimated to have lasted ≤20,000 years. The extinction interval was less than 200,000 years, and synchronous in marine and terrestrial realms; associated charcoal-rich and soot-bearing layers indicate widespread wildfires on land. A massive release of thermogenic carbon dioxide and/or methane may have caused the catastrophic extinction.**

The five major Phanerozoic mass extinctions have been studied for decades, yet the ages and durations of the extinctions and recoveries are generally not well constrained. Detailed timescales for extinctions and recoveries are essential for understanding the physical, ecological, and chemical changes, and for testing possible causes. The end-Permian mass extinction was the most severe in the Phanerozoic, with substantial loss of marine and terrestrial species. Debates about the cause involve evidence for long-lived or rapid anoxia in deep water (*1*–*3*), a major negative excursion in carbon isotopes (*4*–*7*), the approximate coincidence with eruption of the Siberian flood basalts (*8*, *9*) and the subsequent protracted (~5 Myr) biologic recovery (*7*). Models involving bolide impacts (*10*) and catastrophic methane release (*11*) have also been proposed. Recent studies focused on geochemical and biomarker evidence for the development of globally anoxic to euxinic oceans that released $CO_2$ and $H_2S$ into shallow marine settings (*1*, *3*, *12*, *13*), effects on the carbon cycle by the Siberian flood basalts (*14*), and the physiological response of different ecosystems to increased $CO_2$ and $H_2S$ and lowered oxygen (*15*).

Previous analyses of biodiversity across the end-Permian mass extinction are either global compilations with coarse time bins that sacrifice temporal resolving power or studies of single sequences of strata that avoid the problems of correlation and simplify the accounting of species richness, but severely compromise the sampling scope and are susceptible to bias from stratigraphic incompleteness and facies control of preservation. High-precision timescales are fundamental to evaluating the cause of extinction. To achieve sufficient geochronologic constraints, however, dates must be combined from the relatively few sections that contain abundant datable volcanic ash beds and rich information about fossil species and ocean composition. Thus, calibrating a mass extinction requires integration of global signals of the

extinction and environmental change with local geochronologic control.

We present a high-resolution chronology of the end-Permian mass extinction in multiple marine, transitional and terrestrial depositional sections from South China and the peri-Gondwanan region (fig. S1) that is based on integration of a large biodiversity dataset with high-precision geochronologic, biostratigraphic, and $\delta^{13}C$ data. High-resolution chronostratigraphic control and computer-assisted correlation allow us to increase the sampling scope considerably beyond that of single sections without sacrificing their resolving power.

**U-Pb geochronology.** We established a chronology of the end-Permian extinction using U-Pb isotope dilution thermal ionization mass spectrometry (ID-TIMS) on 300 single grains of zircon and monazite from 29 volcanic ash beds in five marine, two marine-terrestrial transitional, and two terrestrial sections in South China (Figs. 1 and 2; tables S1 and S2) (*16*). U-Pb geochronology of zircon from volcanic ash beds interlayered with fossil-bearing carbonate rocks can establish ages with uncertainties of ± 60-120 Kyr (2σ) for 250 Ma rocks. High-resolution ages strengthen the paleontologic correlation between these realms.

Previous estimates of the Permian-Triassic boundary (PTB) range from 251.4 to >254 Ma (*17*–*19*). We dated some samples reported in (*17*) and many new samples from well-known sections in four areas of South China (SOM Text 1; Fig. 1 and fig. S1A; table S1): (1) Meishan with two Global Stratotype Section and Points (GSSPs), (2) Shangsi, (3) Penglaitan and Tieqiao, and (4) several terrestrial and marginal marine sections (figs. S2 to S4). Dates from zircon are $^{206}Pb/^{238}U$ dates based on analyses of single grains *(16)*. $^{207}Pb/^{235}U$ dates from monazite in two samples are used instead of zircon to interpret depositional ages because there is considerable scatter in the zircon dates. The scatter is likely due to slight amounts of inheritance, Pb loss, or an extended period of residence in the magma (tables S1 and S2).

U-Pb dates from this study are considerably more precise than those from previous studies due to enhanced ionization efficiency in the mass spectrometer and a reduction in the amount of common Pb in our zircon analyses [0.48 pg, compared with 4.0 and 1.9 pg in (*17*, *18*), respectively], leading to higher ratios of radiogenic Pb to common Pb. The average 2σ error on the majority of individual $^{206}Pb/^{238}U$ dates that are neither xenocrysts nor contain a xenocrystic component is ± 0.23 Myr (0.09%), smaller than previous average errors on dates of ± 1.0-1.2 Myr (*17*, *18*). The improved precision enhances our ability to identify grains that have suffered slight Pb loss or contain a minor xenocrystic component.

Weighted mean dates from beds 7 and 22 at Meishan are within error of those published in (*17*), but dates from the beds 25 and 28 near the PTB are 0.88 and 1.4 Myr older, respectively. The date from Bed 25 agrees with that in (*18*) and the date from Bed 28 is younger than that in (*19*). Dates from Penglaitan agree with those in (*17*), whereas the date from Heshan is 0.7 Myr older than three dates from (*17*). The discrepancy between our new dates and those of (*17*) are most likely due to Pb loss in grains dated by (*17*) that was not eliminated by mechanical abrasion, but has now been eliminated using chemical abrasion. Dates from Shangsi ash beds at -0.3, -12.8, and -27.4 m below the PTB agree with those from (*18*) and are two to three times more precise. A decay-constant-adjusted $^{207}Pb/^{235}U$ monazite date from -2.9 m agrees with a zircon date from roughly the same interval in (*18*).

**Age and duration of mass extinction.** Because Meishan is the most intensively studied PTB section, we compared geochronologic dates and the carbon isotope record with a well-resolved conodont biostratigraphy (Figs. 2 and S3). The following sequence of events can be distinguished: (1) a 5‰ negative $\delta^{13}C$ isotopic anomaly over 5 cm that starts abruptly within Bed 24e and ends in Bed 25; (2) the main extinction event between beds 24e and 28 (*5*) (Fig. 3); and (3) the PTB marked by the first appearance of *Hindeodus parvus* at the base of Bed 27c, 14 cm above Bed 25. Geochronologic constraints are provided by ash beds at Bed 25 dated at 252.28 ± 0.08 Ma and Bed 28 (located 8 cm above the PTB) dated at 252.10 ± 0.06 Ma.

The duration of the sharp downturn in carbonate carbon isotopes is best estimated using either the sediment accumulation rates from Bed 22 to Bed 25 or Bed 25 to Bed 28. We favor the latter as our previous microstratigraphic study indicates that this part is highly condensed. Assuming constant sediment accumulation rates between beds 25 and 28, we conclude that: (1) the progressive negative downturn in C isotopic composition of 2.4 per mil over 1.79 m preceded the sudden drop in diversity by approximately 90 Kyr; the sharp negative C isotopic anomaly had a duration less than 20 ± 10 Kyr; (2) the main extinction event began in Bed 24e just before 252.28 ± 0.08 Ma (age of Bed 25) at Meishan and lasted no longer than 200 ± 100 Kyr (from Bed 24e to Bed 28), if the extinction interval is confined to beds 25-26, the duration is no longer than 100 Kyr; (3) the PTB is calculated by interpolation to be 252.17 ± 0.06 Ma (Fig. 2); (4) the Wuchiapingian/Changhsingian boundary is calculated by interpolation to be 254.14 Ma based on the ages of ash beds relative to the first occurrence of *Clarkina wangi* at the Shangsi and Meishan sections (fig. S3).

Twelve ash beds dated in this study were collected from the Shangsi section (Fig. 1 and fig. S3, table S1). Beds that best constrain the age of the extinction horizon were 50 cm above it at 252.16 ± 0.09 Ma, 20 cm below it at 252.28 ± 0.13 Ma, and 30 cm below at 252.37 ± 0.08 Ma. The extinction

interval (*18*) is between 252.28 ± 0.13 Ma and 252.16 ± 0.09 Ma, in agreement with the estimate from Meishan. Despite good agreement between the dates from Shangsi beds dated during this study and in (*18*), there is a difference in the interpreted age of the extinction. Their estimate of 252.6 ± 0.2 Ma is in part controlled by the date of an ash bed [Sample SH32 of (*18*)] located 3.4 m above the extinction horizon that overlaps within error with those from immediately below the boundary.

U-Pb dates from all other dated beds near the PTB agree with results from Meishan and Shangsi. The marine-terrestrial transitional section at Zhongzhai contains ash beds that bracket the PTB and a thin coal seam. A bed immediately above the boundary is 252.00 ± 0.08 Ma and a bed 5 cm below is 252.24 ± 0.13 Ma. We identify the boundary as lying just below the base of the upper ash bed (figs. S5 to S7). Therefore, the age of the PTB at Zhongzhai is the same as at Meishan and Shangsi, although diachroneity at the 0.05-0.10 Myr level cannot be ruled out. Dated beds in the other sections are only from below the PTB. Ages from these beds are the same or older than the ages for the PTB at Meishan, Shangsi, and Zhongzhai, and thus are consistent.

**Extinction patterns.** To improve upon a previous species-level analysis based solely on Meishan (*5*), we pooled occurrence data from 18 biostratigraphically well-studied sections. Twelve richly fossiliferous sections from the Late Guadalupian to Early Triassic of South China span shallow water carbonate platform, slope, and basinal habitats (table S3). Six sections from Tibet, Kashmir and Pakistan, record the southern temperate peri-Gondwanan region (*20*). This encompassed 1450 species from 16 fossil groups including cephalopods, brachiopods, foraminifers, fusulinids, conodonts, corals, bivalves, radiolarians, bryozoans, gastropods, ostracods, fish, calcareous algae, spores and pollen, and plant macrofossils. We generated a composite species richness pattern through the Lopingian to Early Triassic (figs. S8 to S10). To calibrate the end-Permian extinction precisely, we project the combined record of dated ashes and species' first- and last-occurrences (FOs and LOs) into the stratal sequence at the most-intensively studied Meishan section. The full scope of the combined dataset is 2,584 serial estimates of species richness across >16 million years (SOM Text 3, fig. S8), of which 640 successive richness estimates occur in the portion of the time series that captures the end-Permian mass extinction.

The diversity data from 18 sections reveal a sharp drop in biodiversity over a very narrow time interval (Fig. 3, figs. S8 to S10). Several ammonoid, bivalve, small foraminifer and brachiopod species survived the extinction but disappeared soon afterwards, accounting for the decreasing diversity in the earliest Triassic. Some spores and pollens in the Earliest Triassic from Meishan and a few new species, such as *Claraia wangi*, *Hypophiceras* sp. etc., produce a trivial rise in diversity immediately after the PTB, but do not change the general trend of overall decreasing diversity. Although the proportional extinction rate stays high in the Early Triassic, the number of extinct species is very low likely indicating continuing environmental deterioration. Raw, per-section and rarefied taxon richness curves based on a wider interval demonstrate lack of significant sampling bias within the narrower interval of study spanning the extinction event, the previously-repeated two- or multiple-stepped extinction derived from Signor-Lipps effect (*21*) is not supported below the 95% confidence threshold and only one significant step remains (Fig. 3, figs. S8 to S10). At Meishan, the main pulse of extinction in beds 24e-28 is associated with and followed by cyanobacterial expansion with anoxic condition; the latter is a global occurrence (*3*, *13*, *14*).

The taxa projected into the Meishan section reinforce the species richness pattern derived from the Meishan pattern alone (*5*) after the Meishan local ranges are extended based on information from other sections that share these taxa (Fig. 3). At Meishan, U-Pb ages for ash beds indicate that the main extinction event began just before 252.28 ± 0.08 Ma (age of Bed 25). After augmentation of information from all of the sections, Meishan constrains the major event to start no earlier than 252.30 Ma and end before 252.10 Ma; i.e. 200 ± 100 Kyr later - an absolute maximum for the duration of the extinction (Figs. 2 and 3).

**Synchronous collapse of the end-Permian tropical terrestrial ecosystem.** There is ongoing debate over whether the marine event coincides precisely with extinctions among plants and terrestrial vertebrates. The *Gigantopteris* floras of the Permian Paleotethys are interpreted as rainforest-type vegetation in the tropical ever-wet climatic zone. The Permian rainforest collapsed across the PTB and recovery was delayed until the Middle Triassic (SOM Text 4) (*22*). Detailed studies in the Karoo Basin of South Africa and Greenland indicated a catastrophic event for terrestrial vegetation and vertebrates in high paleolatitudes (*23*, *24*), but there are few detailed investigations from tropical coastal and terrestrial P-T sections and none are constrained by precise geochronology.

We investigated three terrestrial and two marine/non-marine transitional sections (SOM Text 2; Fig. 4, figs. S1, S5 to S7) on the eastern slope of a large (~300,000 $km^2$) volcanic plateau (fig. S1A) formed by the late Guadalupian eruption of the Emeishan basalt. Correlation of the P-T transition is established by the first occurrence of *Hindeodus parvus* and other conodonts, the negative carbon isotope shift, U-Pb zircon dating of PTB ash beds and magnetostratigraphic data (SOM Text 2; Fig. 4).

At the marine/terrestrial transitional Chuanyan section, the topmost Changhsingian contains a diverse *Gigantopteris*

flora, a 0.32 m-thick coal seam with an ash bed in the middle, an upper ash bed and a pyrite-rich bed with charcoal fragments, pyritized Triassic bivalves and tiny gastropods; these represent high sulfidic input and transported remnants of a coal-forming tropical forest (fig. S5). Coal palynology (14 species in 18 genera) also reveals a typical Late Permian *Gigantopteris* flora. Twenty-six brachiopod species from the Changhsingian having multiple occurrences were used to locate the major marine extinction. Both the stratigraphic range data (figs. S5 and S6A) and the results of 50% confidence interval analysis suggest that the marine mass extinction level overlaps with the last coal and thus the last tropical forest (fig. S7).

Lithofacies suggest the Zhongzhai section was deposited in a slightly more offshore position than the Chuanyan section. Two boundary ash beds bracketing a 3-5 cm coal seam are correlative with those at the Chuanyan section (Fig. 4, figs. S5 and S6B). In the late Changhsingian below the lower ash bed, 121 marine species including abundant brachiopods, bivalves, bryozoans and fusulinids were recorded (SOM Text 2). Up to 75% of the Changhsingian species became extinct within a 40 cm interval below the lower ash bed. Both the stratigraphic range data (fig. S6B) and a 50% confidence interval analysis for 23 species with multiple occurrences (fig. S7B) suggest that the marine mass extinction is coincident with the last coal.

The Lopingian *Gigantopteris* flora in South China consists of 94 genera and 261 species dominated by hygrophilous and thermophilous plant groups such as pecopterids, gigantopterids, lycopsiales and equisetales. They mostly range up to the latest Changhsingian in South China (SOM Text 4). At the Guanbachong section foliar physiognomy analysis of 31 species 0.9 m below the most negative $\delta^{13}C_{org}$ value indicates that plants with large leaves comprise 88% of the flora and 77% have an entire margin; consistent with percentages found in the warm and humid conditions of modern tropical floras. Similar plant-rich horizons are found at the Longmendong, Chahe and Chuanyan sections where latest Permian rocks deposited before the isotopic negative shift contain 95% of Late Permian or Paleozoic-type ferns and pteridosperms and 5% gymnosperm pollen. In the topmost Changhsingian, within the negative shift of carbon isotope, the abundance of fern and pteridosperm spores decreases to 61.2% while gymnosperm pollen increases to 38.8%. At the Longmendong section, 22 species in 23 genera are present in the PTB breccia bed. The immediately overlying lowest Triassic is barren of coal, plant fossils and palynomorphs.

C-isotopic data of organic matter ($\delta^{13}C_{org}$) *(16)* from three terrestrial sections show consistent values of -23 to -24‰ during the Lopingian, followed by sharp drops in $\delta^{13}C_{org}$ ranging from ~5.8‰ to ~10‰ that coincide with mass extinction (Fig. 4). Such a rapid drop in $\delta^{13}C$ slightly below the PTB has been also used to locate the PTB in non-marine sequences in Australia, Antarctica, and South Africa although in the absence of additional biostratigraphic or radiometric data the correlations have been disputed (*4*, *24*). The negative organic C isotope anomaly is apparently younger than 252.30 ± 0.07 Ma based on the age of the underlying ash bed (Chahe 68) in the Chahe section, which is nearly consistent in age with Bed 25 at the Meishan section (Fig. 4; table S4). Palynological study indicates a dramatic reduction of the diversity and abundance of the *Gigantopteris* flora above Bed 68 at the Chahe section (*25*). Thus, the immediately overlying terrestrial extinction is consistent with those at the transitional Zhongzhai and Chuanyan sections and the marine extinction at the Meishan section (*5*). The isotopic negative shift also coincides with the abrupt cessation of coal formation in southern high paleolatitudes (*26*). The $\delta^{13}C_{carb}$ and/or $\delta^{13}C_{org}$ and the floral data in South China suggest that a rapid collapse of the tropical rainforest occurred within the negative shift of $\delta^{13}C_{org}$ very close to the PTB and that the disappearance of the highly-diverse *Gigantopteris* flora is synchronous with the mass extinction of marine organisms (Fig. 4).

**Widespread wildfires.** Evidence of widespread deforestation close to the PTB comes from distinctive charcoal layers with abundant pyrofusinite at several localities in South China (Figs. 4, 5 and fig. S11) *(16)*. Fire-derived products have been recorded from PTB beds at the Meishan section (*13*, *27*). Charcoal layers are also found from horizons correlated biostratigraphically and geochemically to the PTB at the Tieqiao Section in Guangxi, South China and near the PTB in Xinjiang Province and North China (Fig. 5). We interpret the pyrofusinite as transported from environments with charcoal and soot produced by burning of the rainforests in terms of its homogenized cell walls, three-dimensional cellular preservation with open lumina, pitted tracheid and brittle fracture (Fig. 5). Other fire evidence was reported from the PTB beds in marine sections in Western Australia (*28*) and Canadian High Arctic (*29*). The widespread distributions of fire-derived products suggest that dramatic global warming and increasing aridity reached a climax coincident with the marine extinction, rapidly turned the ever-wet biome into a seasonally dry climate and increased forest fire and immediately followed by catastrophic soil erosion (*30*) and fungal virulence (*31*) due to rapid deforestation.

**Causes of the end-Permian mass extinction.** A shift in latest Permian $\delta^{13}C_{carb}$ began with a gradual decline at the base of Bed 23 at Meishan (Fig. 2), which could be interpreted as the collapse of the biological pump (*32*), an increase of continental weathering caused by sea-level fall or massive volcanism (*9*, *17*, *33*). The gradual decline of C

isotopes with a short duration (maximum duration of 90 Kyr) is followed by a brief ≤20 Kyr negative pulse of $\delta^{13}C_{carb}$ associated with the sharp drop of biodiversity between the uppermost part of Bed 24 and Bed 25, which is immediately followed by the negative shift of $\delta^{13}C_{org}$ (Figs. 2 and 3). Dates from Shangsi and Zhongzhai, the two other sections with dated ash beds bracketing the PTB, support this result. Biomarker and organic carbon isotopic studies are consistent with widespread continental weathering and transport of plant fragments and black carbon from wildfires, related to collapse and burning of terrestrial plants (*27*, *30*, *34*). The correlations between marine, marine-terrestrial transitional, and terrestrial sections (Fig. 4) indicate that the marine extinction was synchronous across South China at the <0.2 Myr level with loss of the rainforest, wildfires and the cessation of coal formation (*24*, *26*). Integrated biomarker and organic C isotopic studies also indicate perturbations to the carbon cycle characterized by increased terrestrial weathering during and immediately after the collapse of terrestrial ecosystem and widespread introduction of sulfidic waters into the photic zone (*1*, *12*, *33*) as indicated by the concentration of pyrite within the extinction horizon and cyanobacterial expansion (*13*).

Despite evidence for dysoxic and anoxic conditions in the deep ocean both just before and after the extinction (*2*, *3*), the synchroneity of $C_{carb}$ isotope excursion and extinction suggest a causal link between the introduction of the light carbon and the extinction. The simplest way to produce a widespread, large pulse of shallow water anoxia and euxinia is by carbon dioxide and/or methane-induced global warming that leads to decreased oxygen solubility, intensification of continental weathering, and increased nutrient delivery to the oceans [e.g., (*33*)] with biodiversity decline coinciding with onset of a period of rapid warming.

The data presented here allows us to better constrain such hypotheses. The $\delta^{13}C_{carb}$ drops about 7‰ over roughly 100 Kyr, and about 5‰ in roughly the last 10 Kyr of those 100 Kyr, with the $\delta^{13}C_{org}$ decline immediately after the decline in $\delta^{13}C_{carb}$. An understanding of such fast changes requires a model of isotopic evolution that explicitly considers rates of change. Here we use our new time scale to calculate how much additional light carbon of a fixed composition $\delta_i$ must be added to the system to reproduce the excursion as seen at Meishan, under the assumption that the isotopic changes occur in globally well-mixed oceans. The result provides the mass $m'$ of additional light carbon, normalized by the assumed pre-existing size $m^*$ of the oceans' reservoir of dissolved inorganic carbon (DIC) (fig. S12). As expected, lighter inputs require less flux. However, no known worldwide reservoir of light organic carbon contains greater than about 5000 Gt (*35*). The modern value for DIC, on the other hand, suggests $m^* \approx 38000$ Gt (*36*). Thus the maximum conceivable modern value of $m'/m^*$ is about 0.13, somewhat less than the value of 0.16 that would be required for methane hydrates ($\delta_i$ = -60‰), and much less than the value of 0.38 required from typical organic carbon ($\delta_i$ = -28‰). Neither comparison disqualifies the scenario of a massive injection of light carbon. It instead indicates the unusual nature of the end-Permian environment.

The end-Permian extinction has long been linked to eruption of the massive Siberian flood basalts through production of large amounts of sulfates, $CO_2$ and possibly thermogenic methane (*8*, *9*, *13*, *14*, *29*, *33*, *37*). A previous U-Pb study of the flood basalts (*8*) shows that much of them are slightly younger than our interpreted extinction age. The age discrepancy could be due to interlaboratory bias related to calibration of the tracer solutions used in different laboratories. Mundil et al. (*18*) combined recalculated $^{40}Ar$-$^{39}Ar$ dates for Bed 25 from Meishan (252.1 ± 1.6 Ma) with the earlier study showing $^{40}Ar$-$^{39}Ar$ dates of flood basalts and Bed 25 are the same age (*9*) to conclude that the flood basalts and extinction are essentially synchronous. Recent work has focused on the role of large intrusions of basaltic magmas that have interacted with organic rich shales and petroleum-bearing evaporites that may have caused large quantities of greenhouse gases to be released at 252.0 ± 0.4 Ma (*38*).

Our studies indicate that both marine and terrestrial ecosystems collapsed very suddenly and massive release of thermogenic $CO_2$, as well as methane is a highly plausible explanation (*29*, *39*). Our data on the timing and pace of the end-Permian mass extinction are consistent with rapid $CO_2$ increase as indicated by distinct paleophysiologic effects of the ecosystem (*15*), a sharp drop in $O_2$ (*40*) and substantial addition of atmospheric sulphate-bearing aerosols. These critical inputs could have resulted in an increase in continental aridity by rapid global warming, which caused widespread wildfires and accelerated deforestation in the world. Rapid deforestation further enhanced the continental weathering and finally resulted in a catastrophic soil-erosion on the continent at PTB (*30*).

**References and Notes**


1. C. Q. Cao *et al.*, *Earth Planet. Sci. Lett.* **281**, 188 (2009).
2. Y. Isozaki, *Science* **276**, 235 (1997).
3. G. A. Brennecka, A. D. Herrmann, T. J. Algeo, A. D. Anbar, *Proc. Natl. Acad. Sci.* DOI: 10.1073/pnas.1106039108 (2011).
4. M. J. de Wit *et al.*, *J. Geol.* **110**, 227 (2002).
5. Y. G. Jin *et al.*, *Science* **289**, 432 (2000).
6. E. S. Krull *et al.*, *Palaeogeog. Palaeoclimat. Palaeoecol.* **204**, 297 (2004).
7. J. L. Payne *et al.*, *Science* **305**, 506 (2004).
8. S. L. Kamo *et al.*, *Earth Planet. Sci. Lett.* **214**, 75 (2003).
9. P. R. Renne, Z. C. Zhang, M. A. Richards, M. T. Black, A. R. Basu, *Science* **269**, 1413 (1995).

10. L. Becker, R. J. Poreda, A. G. Hunt, T. E. Bunch, M. Rampino, *Science* **291**, 1530 (2001).
11. D. H. Erwin, *The Great Paleozoic Crisis: Life and death in the Permian* (Columbia Univ. Press, New York, 1993).
12. K. Grice *et al.*, *Science* **307**, 706 (2005).
13. S. C. Xie *et al.*, *Geology* **35**, 1083 (2007).
14. J. L. Payne *et al.*, *Geol. Soc. Am. Bull.* **119**, 771 (2007).
15. A. H. Knoll, R. K. Bambach, J. L. Payne, S. Pruss, W. W. Fischer, *Earth Planet. Sci. Lett.* **256**, 295 (2007).
16. Materials and methods are available on *Science* Online.
17. S. A. Bowring *et al.*, *Science* **280**, 1039 (1998).
18. R. Mundil, K. R. Ludwig, I. Metcalfe, P. R. Renne, *Science* **305**, 1760 (2004).
19. R. Mundil *et al.*, *Earth Planet. Sci. Lett.* **187**, 131 (2001).
20. S. Z. Shen *et al.*, *Palaeoworld* **15**, 3 (2006).
21. H. F. Yin, Q. L. Feng, X. L. Lai, A. Baud, J. N. Tong, *Global Planet. Change* **55**, 1.
22. C. V. Looy, R. J. Twitchett, D. L. Dilcher, J. H. A. Konijnenburg-Van Cittert, H. Visscher, *Proc. Natl. Acad. Sci. USA* **98**, 7879 (2001).
23. R. J. Twitchett, C. V. Looy, R. Morante, H. Visscher, P. B. Wignall, *Geology* **29**, 351 (2001).
24. P. D. Ward *et al.*, *Science* **307**, 709 (2005).
25. Y. Q. Peng, J. X. Yu, Y. Q. Gao, F. Q. Yang, *J. Asian Earth Sci.* **28**, 291 (2006).
26. G. J. Retallack, J. J. Veevers, R. Morante, *Geol. Soc. Am. Bull.* **108**, 195 (1996).
27. W. J. Shen, Y. G. Sun, Y. T. Lin, D. H. Liu, P. X. Chai, *Geochim. Cosmochim. Acta* **75**, 1992 (2011).
28. B. M. Thomas *et al.*, *Aust. J. Earth Sci.* **51**, 423 (2004).
29. S. E. Grasby, H. Sanei, B. Beauchamp, *Nature Geoscience* **4**, 104 (2011).
30. M. A. Sephton *et al.*, *Geology* **33**, 941 (2005).
31. H. Visscher, M. A. Sephton, C. V. Looy, *Geology* **39**, 883 (2011).
32. A. Riccardi, L. R. Kump, M. A. Arthur, S. D'Hondt, *Palaeogeog. Palaeoclimat. Palaeoecol.* **248**, 73 (2007).
33. T. J. Algeo, Z. Q. Chen, M. L. Fraiser, R. J. Twitchett, *Palaeogeog. Palaeoclimat. Palaeoecol.* **308**, 1 (2011).
34. B. Nabbefeld, K. Grice, R. E. Summons, L. E. Hays, C. Q. Cao, *Appl. Geochem.* **25**, 1374 (2010).
35. A. V. Milkov, *Earth-Sci. Rev.* **66**, 183 (2004).
36. W. T. Holser, M. Schidlowski, F. T. Mackenzie, J. B. Maynard, in *Chemical Cycles in the Evolution of the Earth,* C. B. Gregor, R. M. Garrels, F. T. Mackenzie, J. B. Maynard, Eds. (John Wiley & Sons, New York, 1988), pp. 105-173.
37. D. H. Erwin, *Extinction* (Princeton Univ. Press, Princeton, NJ (2005).
38. H. Svensen *et al.*, *Earth Planet. Sci. Lett.* **277**, 490 (2009).
39. G. J. Retallack, A. H. Jahren, *J. Geol.* **116**, 1 (2008).
40. R. B. Huey, P. D. Ward, *Science* **308**, 398 (2005).
41. B. Schoene, J. L. Crowley, D. J. Condon, M. D. Schmitz, S. A. Bowring, *Geochim. Cosmochim. Acta* **70**, 426 (2006).
42. J. M. Mattinson, *Chem. Geol.* **220**, 47 (2005).
43. J. S. Stacey, J. D. Kramers, *Earth Planet. Sci. Lett.* **26**, 207 (1975).
44. A. H. Jaffey, K. F. Flynn, L. E. Glendenin, W. C. Bentley, A. M. Essling, *Physical Review C* **4**, 1889 (1971).
45. M. D. Schmitz, B. Schoene, *Geochem. Geophy. Geosy.* **8**, 1 (2007).
46. U. Schärer, *Earth Planet. Sci. Lett.* **67**, 191 (1984).
47. K. R. Ludwig, *Isoplot/EX version 3.0, A geochronological toolkit for Microsoft Excel.*, Berkeley Geochronology Center Special Publication, No. 4 (Berkeley Geochronology Center Berkeley, 2003), pp. 71.
48. J. I. Simon, P. R. Renne, R. Mundil, *Earth Planet. Sci. Lett.* **266**, 182 (2008).
49. C. Q. Cao, W. Wang, Y. G. Jin, *Chinese Sci. Bull.* **47**, 1125 (2002).
50. Z. S. Li *et al.*, *Study on the Permian-Triassic biostratigraphy and event stratigraphy of northern Sichuan and southern Shaanxi*. People's Republic of China Ministry of Geology and Mineral Resources, Geological Memoirs, Ser. 2, no. 9 (Geological Publishing House, Beijing, 1989).
51. T. W. Boutton, in *Carbon isotope techniques,* D. C. Coleman, B. Fry, Eds. (Academic, San Diego, 1991), pp. 173-195.
52. M. Magaritz, R. V. Krishnamurthy, W. T. Holser, *Am. J. Sci.* **292**, 727 (1992).
53. J. M. McCrea, *J. Chem. Phy.* **18**, 849 (1950).
54. A. C. Scott, *Int. J. Coal Geol.* **12**, 443 (1989).
55. C. Q. Cao, Q. F. Zheng, *J. Stratigraphy* **31**, 14 (2007).
56. S. Z. Shen, Y. Wang, C. M. Henderson, C. Q. Cao, W. Wang, *Palaeoworld* **16**, 120 (2007).
57. Y. Zeng, *J. China Coal Soc.* **15**, 41 (1990).
58. Y. Q. Peng *et al.*, *Palaeogeog. Palaeoclimat. Palaeoecol.* **215**, 285 (2005).
59. J. X. Yu *et al.*, *Global Planet. Change* **55**, 193 (2007).
60. Y. Q. Peng, G. R. Shi, *Global Planet. Change* **65**, 155 (2008).
61. L. T. Wang, Y. B. Lu, S. J. Zhao, H. Luo, *Permian lithofacies paleogeography and mineralization in South China*. H. Z. Wang, Z. Z. Ye, S. C. Guan, Y. F. Zeng, Eds., Book series on lithofacies and paleogeography in South China (Geological Publishing House, Beijing, 1994).
62. T. J. Algeo, B. Ellwood, T. K. T. Nguyen, H. Rowe, J. B. Maynard, *Palaeogeog. Palaeoclimat. Palaeoecol.* **252**, 304 (2007).
63. A. Arche, J. Lopez-Gomez, *Palaeogeog. Palaeoclimat. Palaeoecol.* **229**, 104 (2005).

64. G. J. Retallack, *J. Sediment. Res.* **75**, 679 (2005).
65. A. Sandler, Y. Eshet, B. Schilman, *Palaeogeog. Palaeoclimat. Palaeoecol.* **242**, 68 (2006).
66. I. Metcalfe, R. S. Nicoll, *Palaeogeog. Palaeoclimat. Palaeoecol.* **252**, 56 (2007).
67. S. Y. Wang, H. F. Yin, *Study on terrestrial Permian-Triassic boundary in eastern Yunnan and western Guizhou*. (China University of Geosciences Press, Wuhan, 2001), pp. 88.
68. J. M. G. Glen *et al.*, *J. Asian Earth Sci.* **36**, 521 (2009).
69. F. Heller, W. Lowrie, H. Li, J. Wang, *Earth Planet. Sci. Lett.* **88**, 348 (1988).
70. M. Steiner, J. Ogg, Z. K. Zhang, S. Sun, *J. Geophy. Res.* **94**, 7343 (1989).
71. X. H. Ma, M. W. McElhinny, B. J. J. Embleton, Z. K. Zhang, *Geophys. J. Int.* **114**, 293 (1993).
72. M. Haag, F. Heller, *Earth Planet. Sci. Lett.* **107**, 42 (1991).
73. H. M. Li, J. D. Wang, *Science in China Ser. B* **32**, 1402 (1989).
74. Y. Y. Liu, Y. M. Zhu, W. H. Tian, *Earth Science-J. China Univ. Geosciences* **24**, 151 (1999).
75. M. Szurlies, *Earth Planet. Sci. Lett.* **261**, 602 (2007).
76. B. A. Marshall, *J. Roy. Soc. New Zeal.* **25**, 495 (1995).
77. C. R. Marshall, *Paleobiology* **16**, 1 (1990).
78. C. R. Marshall, *Geology* **23**, 731 (1995).
79. C. R. Marshall, *Paleobiology* **23**, 165 (1997).
80. S. C. Wang, C. R. Marshall, *Paleobiology* **30**, 5 (2004).
81. P. M. Sadler, *Annu. Rev. Earth Planet. Sci.* **32**, 187 (2004).
82. P. M. Sadler, *Paleontological Society Papers* **16**, 271 (2010).
83. D. J. Strauss, P. M. Sadler, *Math. Geol.* **21**, 411 (1989).
84. C. R. Marshall, *Paleontological Society Papers* **16**, 291 (2010).
85. P. M. Sadler, R. A. Cooper, in *High Resolution Approaches in Paleontology,* P. J. Harries, Ed. (Kluwer-Academic Press, Dordrecht, 2003), pp. 49-94.
86. Z. Q. Yao, J. T. Xu, S. G. Zheng, X. F. Zhao, Z. G. Mu, in *Late Permian coal-bearing stratigraphy and biota in western Guizhou and eastern Yunnan area,* Nanjing Institute of Geology and Palaeontology, Ed. (Science Press, Beijing, 1980), pp. 1-69.
87. G. R. Shen, in *Fossil floras of China through the geological ages,* X. X. Li, Ed. (Guangdong Science and Technology Press, Guangzhou, 1995), pp. 1-695.
88. X. L. He, D. S. Liang, S. Z. Shen, *Research on the Permian flora from Jiangxi Province, China*. (China Univ. of Mining & Technology Press, Xuzhou, 1996), pp. 300.
89. C. H. Xiong, Q. Wang, *Paleobiology* **37**, 157 (2011).
90. A. C. Scott, I. J. Glasspool, *Geology* **33**, 589 (2005).
91. Y. Wang, Y. G. Jin, *Palaeogeog. Palaeoclimat. Palaeoecol.* **160**, 35 (2000).
92. A. M. Ziegler, M. L. Hulver, D. B. Rowley, in *Late glacial and postglacial environmental changes--Quaternary, Carboniferous-Permian and Proterozoic,* I. P. Martini, Ed. (Oxford University Press, New York, 1997), pp. 111-146.
93. S. L. Mei, C. M. Henderson, C. Q. Cao, *Geological Society Special Publications* **230**, 105 (2004).
94. S. Z. Shen, S. L. Mei, *Geol. J.* **45**, 135 (2010).
95. J. Chen, T. W. Beatty, C. M. Henderson, H. D. Rowe, *J. Asian Earth Sci.* **36**, 442 (2009).
96. Y. G. Jin *et al.*, *Episodes* **29**, 253 (2006).
97. Y. G. Jin *et al.*, *Episodes* **29**, 175 (2006).
98. H. F. Yin, K. X. Zhang, J. N. Tong, Z. Y. Yang, S. B. Wu, *Episodes* **24**, 275 (2001).
99. H. L. Hsieh, L. A. Li, *Zoological Studies* **37**, 13 (1998).
100. H. Song, J. Tong, Z. Q. Chen, *Aust. J. Earth Sci.* **56**, 765 (2009).
101. Q. L. Feng *et al.*, *Global Planet. Change* **55**, 177 (2007).
102. S. C. Xie, R. D. Pancost, H. F. Yin, H. M. Wang, R. P. Evershed, *Nature* **434**, 494 (2005).
103. D. H. Rothman, J. M. Hayes, R. E. Summons, *Proc. Natl. Acad. Sci. USA* **100**, 8124 (2003).
104. Y. Wang *et al.*, *J. Asian Earth Sci.* **26**, 575 (2006).
105. K. X. Zhang, J. X. Yu, Q. X. Lin, Y. L. Jiang, B. Chen, *Earth Science-J. China Univ. Geosciences* **29**, 253 (2004).
106. J. N. Tong, H. J. Hansen, L. S. Zhao, J. X. Zuo, *J. Stratigraphy* **29**, 205 (2005).
107.Z. Y. Yang *et al.*, *Permian-Triassic boundary stratigraphy and fauna of South China*. PRC Ministry of Geology and Mineral Resources, Geological Memoirs, Ser. 2, no. 6 (Geoligical Publishing House, Beijing, 1987), pp. 379.
108. M. Nafi, W. C. Xia, N. Zhang, *Can. J. Earth Sci.* **43**, 121 (2006).
109. W. H. He, S. Z. Shen, Q. L. Feng, S. Z. Gui, *J. Paleontol.* **79**, 927 (2005).
110. Q. H. Shang, M. Caridroit, Y. J. Wang, *Acta Micropalaeontologica Sinica* **18**, 229 (2001).
111. S. Z. Shen *et al.*, *Global Planet. Change* **73**, 3 (2010).

**Acknowledgements.** This research is supported by NSFC, the National Basic Research Program of China (2006CB806400, 2011CB808905), the CAS/SAFEA International Partnership Program, CAS grants #KZCX2-YW-Q08-4 and #BK2010022 of basic research program of Jiangsu Province for the Nanjing Group. Further support was provided by a U.S. National Aeronautics and Space Administration (NASA) Astrobiology Institute Grant for SAB and DHE, NASA Exobiology Program grant #NNX09AM88G for CQC, NASA Grant #NNA08CN84A for DHR and a NSER Discovery Grant for CMH. All data

are available in the Supporting Online Material. **Author contributions.** This paper is dedicated to Prof. Y.G. Jin who initiated the China-US joint research with S.A. Bowring and D.H. Erwin. S.A. Bowring, D.H. Erwin, S.Z. Shen and Y. Wang wrote the paper with inputs from J.L. Crowley, C.M. Henderson, D.H. Rothman and P.M. Sadler. All geochronologic ages were produced by S.A. Bowring and J.L. Crowley. Diversity pattern analysis using CONOP were carried out by Y. Wang and P.M. Sadler with the database established by Y. Wang and S.Z. Shen. Biostratigraphy was analyzed by S.Z. Shen, C.M. Henderson and Y. Wang. Carbon isotope dynamic model based on the Meishan section was conducted by D.H. Rothman with the data from C.Q. Cao. All data from the terrestrial and transitional sections were analyzed by S.Z. Shen and other co-authors of the Nanjing group. All authors joined in field work and contributed to the interpretation of the data.

**Supporting Online Material**
www.sciencemag.org/cgi/content/full/science.1213454/DC1
Materials and Methods
SOM Text
Figs. S1 to S12
Tables S1 to S4
References (*41–111*)

1 September 2011; accepted 28 October 2011
Published online 17 November 2011;
10.1126/science.1213454

**Fig. 1.** Zircon $^{206}Pb/^{238}U$ and monazite $^{207}Pb/^{235}U$ dates from volcanic ash beds from South China including five marine, two transitional and two terrestrial sections. Sample numbers, distances from PTB and ages are given in table S1 and SOM Text 1.

**Fig. 2.** Meishan section showing carbonate and organic C isotope data from core and outcrop (*1*), and $^{206}Pb/^{238}U$ zircon ages of ash beds. Stratigraphic column is scaled in time, which affects the appearance of the exact same data scaled to meters in Fig. 3. Arrows indicate the negative excursions of carbon isotopes.

**Fig. 3.** Composite taxon richness, geochronometry and carbon isotope data mapped into the PTB interval of the Meishan section. 1, Taxon richness based solely on ranges observed in the Meishan section. 2, Taxon richness after extension of those observed ranges to fit CONOP composite sequence for all sections. 3, Taxon richness after addition of ranges for taxa seen only at other sections. Solid arrows and red bold font are dated horizons at Meishan. Dashed arrows and italic font are some dated key horizons at other sections projected into Meishan sample horizons by CONOP compositing algorithms according to the associated fossil taxa. Vertical bars on x-axis: position of sample horizons at Meishan. The dates are U-Pb zircon $^{206}Pb/^{238}U$ and monazite $^{207}Pb/^{235}U$ ages of ash beds. Carbon isotope data are from (*1*).

**Fig. 4.** Correlation of the disappearance of the *Gigantopteris* flora, charcoal layers, lithologic color shift and carbon isotope excursions between the terrestrial and transitional PTB sequences on the eastern slope of the Emeishan volcanic plateau and the marine Meishan Section. Dashed blue line represents the correlated position between the stratigraphic sections which is just above the major extinction pulse. The carbon isotope profile at the Meishan Section is after (*1*). The dates are U-Pb zircon $^{206}Pb/^{238}U$ ages of ash beds. Color of the lithology approximately represents the Munsell color of rocks measured in the field.

**Fig. 5.** Scanning electron micrographs of charcoal and carbon micro-particles from the PTB beds in South China. (**A**) transverse view of a fragment of charcoal from Guanbachong showing homogenized cell walls and three-dimensional cellular preservation with open lumina. (**B**) showing pitted tracheid with spiral lines, from Guanbachong. (**C**) from the *Clarkina meishanensis* Zone just below the PTB at the Tieqiao section in Laibin, Guangxi Province. (**D**) showing homogenization of cell walls, pitted tracheid and brittle fracture from Chuanyan section. (**E**) Carbon particle from Bed 25 at Meishan C section. White bars=20μm.

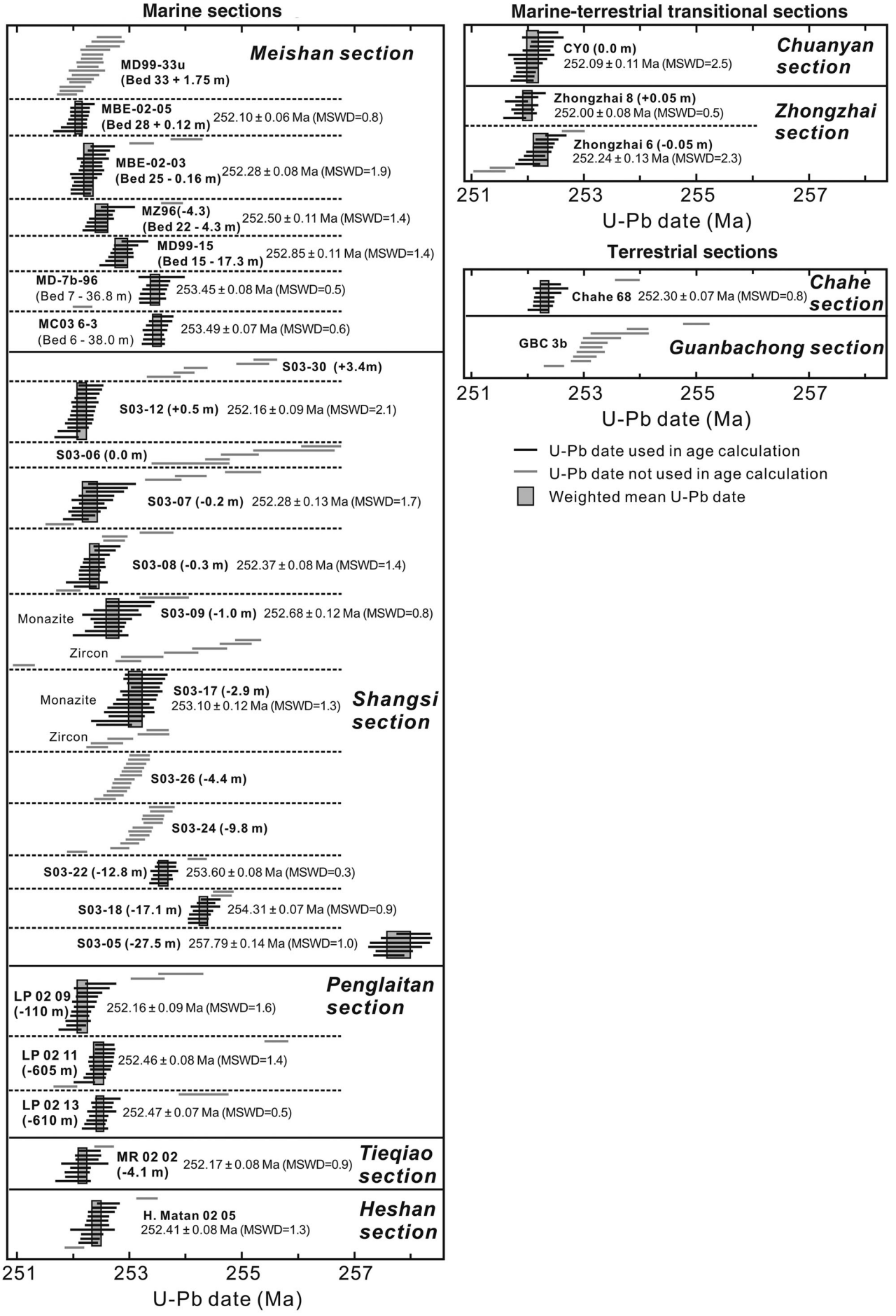
Marine sections
Meishan section
MD99-33u
(Bed 33 + 1.75 m)
MBE-02-05
(Bed 28 + 0.12 m)
252.10 ± 0.06 Ma (MSWD=0.8)
MBE-02-03
(Bed 25 - 0.16 m)
252.28 ± 0.08 Ma (MSWD=1.9)
MZ96(-4.3)
(Bed 22 - 4.3 m)
252.50 ± 0.11 Ma (MSWD=1.4)
MD99-15
(Bed 15 - 17.3 m)
252.85 ± 0.11 Ma (MSWD=1.4)
MD-7b-96
(Bed 7 - 36.8 m)
253.45 ± 0.08 Ma (MSWD=0.5)
MC03 6-3
(Bed 6 - 38.0 m)
253.49 ± 0.07 Ma (MSWD=0.6)
S03-30 (+3.4m)
S03-12 (+0.5 m) 252.16 ± 0.09 Ma (MSWD=2.1)
S03-06 (0.0 m)
S03-07 (-0.2 m) 252.28 ± 0.13 Ma (MSWD=1.7)
S03-08 (-0.3 m) 252.37 ± 0.08 Ma (MSWD=1.4)
Monazite
S03-09 (-1.0 m) 252.68 ± 0.12 Ma (MSWD=0.8)
Zircon
Monazite
S03-17 (-2.9 m)
253.10 ± 0.12 Ma (MSWD=1.3)
Zircon
Shangsi section
S03-26 (-4.4 m)
S03-24 (-9.8 m)
S03-22 (-12.8 m) 253.60 ± 0.08 Ma (MSWD=0.3)
S03-18 (-17.1 m) 254.31 ± 0.07 Ma (MSWD=0.9)
S03-05 (-27.5 m) 257.79 ± 0.14 Ma (MSWD=1.0)
Penglaitan section
LP 02 09
(-110 m)
252.16 ± 0.09 Ma (MSWD=1.6)
LP 02 11
(-605 m)
252.46 ± 0.08 Ma (MSWD=1.4)
LP 02 13
(-610 m)
252.47 ± 0.07 Ma (MSWD=0.5)
MR 02 02
(-4.1 m)
252.17 ± 0.08 Ma (MSWD=0.9)
Tieqiao section
H. Matan 02 05
252.41 ± 0.08 Ma (MSWD=1.3)
Heshan section
251
253
255
257
U-Pb date (Ma)
Marine-terrestrial transitional sections
CY0 (0.0 m)
252.09 ± 0.11 Ma (MSWD=2.5)
Chuanyan section
Zhongzhai 8 (+0.05 m)
252.00 ± 0.08 Ma (MSWD=0.5)
Zhongzhai 6 (-0.05 m)
252.24 ± 0.13 Ma (MSWD=2.3)
Zhongzhai section
251
253
255
257
U-Pb date (Ma)
Terrestrial sections
Chahe 68 252.30 ± 0.07 Ma (MSWD=0.8)
Chahe section
GBC 3b
Guanbachong section
251
253
255
257
U-Pb date (Ma)
U-Pb date used in age calculation
U-Pb date not used in age calculation
Weighted mean U-Pb date

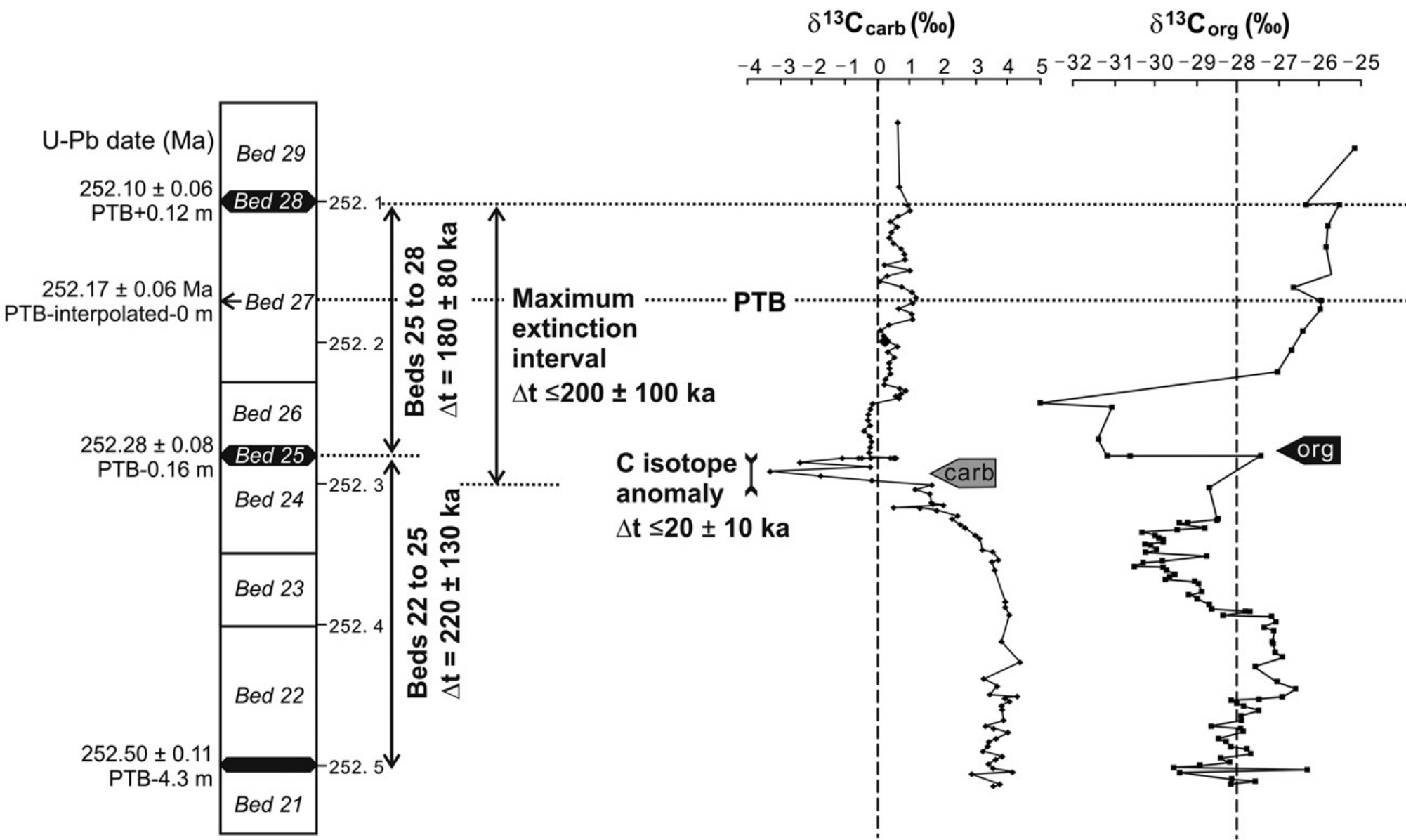
U-Pb date (Ma)
Bed 29
252.10 ± 0.06
PTB+0.12 m
Bed 28
252. 1
252.17 ± 0.06 Ma
PTB-interpolated-0 m
Bed 27
252. 2
Bed 26
252.28 ± 0.08
PTB-0.16 m
Bed 25
252. 3
Bed 24
Bed 23
252. 4
Bed 22
252.50 ± 0.11
PTB-4.3 m
252. 5
Bed 21
Beds 25 to 28
Δt = 180 ± 80 ka
Beds 22 to 25
Δt = 220 ± 130 ka
Maximum
extinction
interval
Δt ≤200 ± 100 ka
PTB
C isotope
anomaly
Δt ≤20 ± 10 ka
δ13Ccarb (‰)
−4 −3 −2 −1 0 1 2 3 4 5
carb
δ13Corg (‰)
−32 −31 −30 −29 −28 −27 −26 −25
org

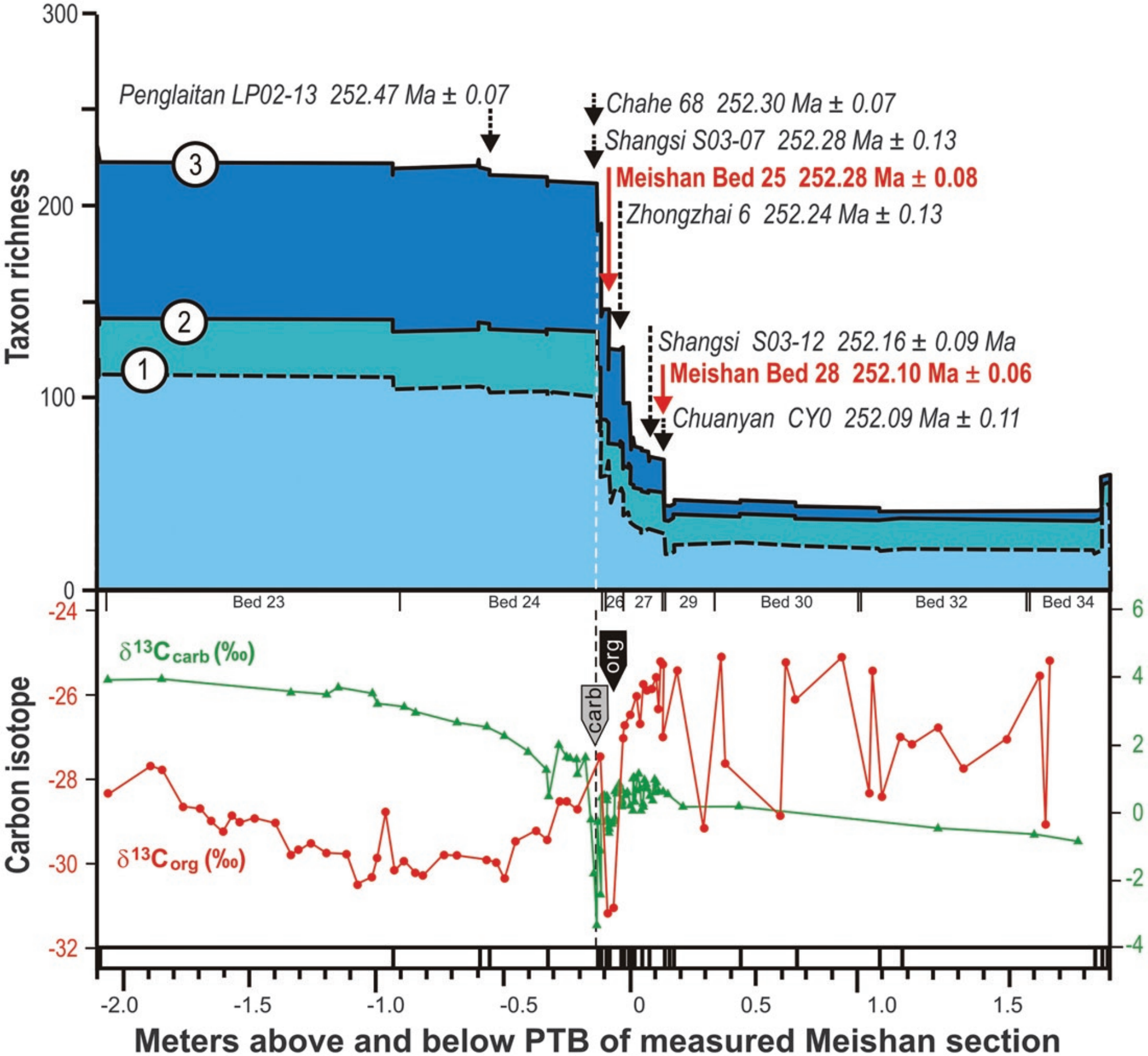
Penglaitan LP02-13 252.47 Ma ± 0.07
Chahe 68 252.30 Ma ± 0.07
Shangsi S03-07 252.28 Ma ± 0.13
Meishan Bed 25 252.28 Ma ± 0.08
Zhongzhai 6 252.24 Ma ± 0.13
Shangsi S03-12 252.16 ± 0.09 Ma
Meishan Bed 28 252.10 Ma ± 0.06
Chuanyan CY0 252.09 Ma ± 0.11
Taxon richness
300
200
100
0
3
2
1
Bed 23
Bed 24
26
27
29
Bed 30
Bed 32
Bed 34
Carbon isotope
δ13Ccarb (‰)
δ13Corg (‰)
carb
org
-24
-26
-28
-30
-32
6
4
2
0
-2
-4
-2.0
-1.5
-1.0
-0.5
0
0.5
1.0
1.5
Meters above and below PTB of measured Meishan section

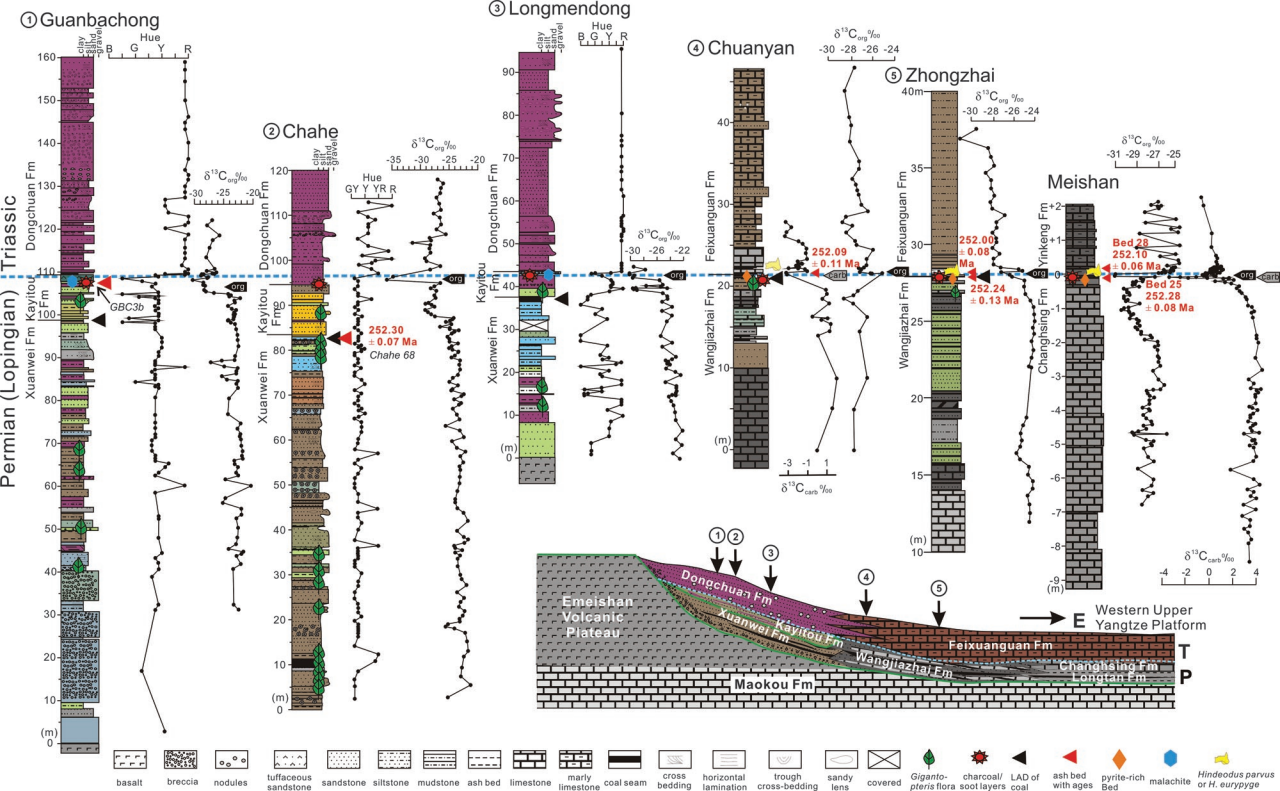
① Guanbachong
② Chahe
③ Longmendong
④ Chuanyan
⑤ Zhongzhai
Meishan
Permian (Lopingian)
Triassic
Dongchuan Fm
Kayitou Fm
Xuanwei Fm
Feixuanguan Fm
Wangjiazhai Fm
Yinkeng Fm
Changhsing Fm
GBC3b
252.30 ± 0.07 Ma
Chahe 68
252.09 ± 0.11 Ma
252.00 ± 0.08 Ma
252.24 ± 0.13 Ma
Bed 28 252.10 ± 0.06 Ma
Bed 25 252.28 ± 0.08 Ma
org
carb
Emeishan Volcanic Plateau
Maokou Fm
Longtan Fm
Western Upper Yangtze Platform
basalt
breccia
nodules
tuffaceous sandstone
sandstone
siltstone
mudstone
ash bed
limestone
marly limestone
coal seam
cross bedding
horizontal lamination
trough cross-bedding
sandy lens
covered
Gigantopteris flora
charcoal/ soot layers
LAD of coal
ash bed with ages
pyrite-rich Bed
malachite
Hindeodus parvus or H. eurypyge

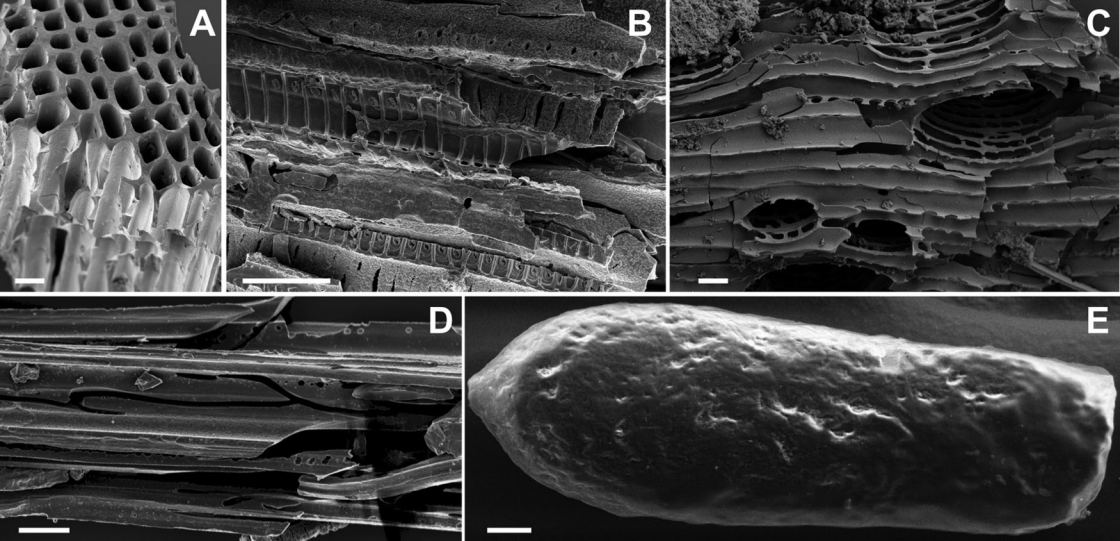
A
B
C
D
E